J|A|C|S ARTICLES

Published on Web 01/23/2009

Adsorption-Driven Surface Segregation of the Less Reactive Alloy Component

Klas J. Andersson,[†] Federico Calle-Vallejo,[‡] Jan Rossmeisl,[‡] and Ib Chorkendorff*,[†]

Center for Individual Nanoparticle Functionality (CINF) and Center for Atomic-Scale Materials Design (CAMD), Department of Physics, NanoDTU, Technical University of Denmark, DK-2800 Kgs. Lyngby, Denmark

Received November 13, 2008; E-mail: ibchork@fysik.dtu.dk

Abstract: Counterintuitive to expectations and all prior observations of adsorbate-induced surface segregation of the more reactive alloy component (the one forming the stronger bond with the adsorbate), we show that CO adsorption at elevated pressures and temperatures pulls the less reactive Cu to the surface of a CuPt near-surface alloy. The Cu surface segregation is driven by the formation of a stable self-organized CO/CuPt surface alloy structure and is rationalized in terms of the radically stronger Pt−CO bond when Cu is present in the first surface layer of Pt. The results, which are expected to apply to a range of coinage (Cu, Ag)/Pt-group bimetallic surface alloys, open up new possibilities in selective and dynamical engineering of alloy surfaces for catalysis.

1. Introduction

Bimetallic alloys offer a way of tuning electronic structure and catalytic properties of metal surfaces.[1−6] Crucial to the catalytic performance of an alloy surface is its composition and structure. The bonding of adsorbates may induce changes in local atomic composition and surface structure, changing the activity and selectivity of the catalyst. Capitalizing on such effects for catalyst preparation means greater flexibility in alloy surface design for low-temperature applications. The expected response to adsorbates is that the more reactive alloy component (i.e., the one forming the strongest chemical bond with the adsorbates) segregates to the surface.[7−14] Counterintuitive to this picture, we show that CO adsorption induces surface segregation of the *less* reactive alloy component, Cu, switching a CuPt *near-surface* alloy[15] to a novel well-ordered CuPt *surface* alloy. This provides a new tool for selective and dynamical CuPt alloy surface engineering as, illustrated in Figure 1. The near-surface and surface alloys are hereafter denoted NSA and SA, respectively.

Figure 1. Illustration of (left) the CuPt NSA and (right) CO-induced Cu surface segregation and the novel SA resulting from it.

The CuPt NSA was recently suggested as a promising water-gas shift ($CO + H_2O \rightarrow H_2 + CO_2$) catalyst because of reduced Pt−CO bonding on a Pt catalyst surface with Cu present in the second layer,[15] alleviating possible CO-poisoning problems.[16] Expanding our work on the Cu/Pt(111) system,[17,18] we show that the NSA is unstable at elevated CO pressures and sample temperatures, forming instead a self-organized CO/CuPt SA

[†] Center for Individual Nanoparticle Functionality (CINF).
[‡] Center for Atomic-Scale Materials Design (CAMD).

(1) Sinfelt, J. *Bimetallic Catalysts: Discoveries, Concepts and Applications*; Wiley: New York, 1983.
(2) Besenbacher, F.; Chorkendorff, I.; Clausen, B. S.; Hammer, B.; Molenbroek, A. M.; Nørskov, J. K.; Steensgaard, I. *Science* **1998**, *279*, 1913–1915.
(3) Greeley, J.; Jaramillo, T. F.; Bonde, J.; Chorkendorff, I.; Nørskov, J. K. *Nat. Mater.* **2006**, *5*, 909–913.
(4) Chen, M.; Kumar, D.; Yi, C.-W.; Goodman, D. W. *Science* **2005**, *310*, 291–293.
(5) Studt, F.; Abild-Pedersen, F.; Bligaard, T.; Sørensen, R. Z.; Christensen, C. H.; Nørskov, J. K. *Science* **2008**, *320*, 1320–1322.
(6) Jacobsen, C. J. H.; Dahl, S.; Clausen, B. S.; Bahn, S.; Logadottir, A.; Nørskov, J. K. *J. Am. Chem. Soc.* **2001**, *123*, 8404–8405.
(7) Shu, J.; Bongondo, B. E. W.; Grandjean, B. P. A.; Adnot, A.; Kaliaguine, S. *Surf. Sci.* **1993**, *291*, 129–138. Gonzalez, S.; Neyman, K. M.; Shaikhutdinov, S.; Freund, H. J.; Illas, F. *J. Phys. Chem. C* **2007**, *111*, 6852–6856.
(8) Christoffersen, E.; Stoltze, P.; Nørskov, J. K. *Surf. Sci.* **2002**, *505*, 200–214.
(9) Menning, C. A.; Hwu, H. H.; Chen, J. G. G. *J. Phys. Chem. B* **2006**, *110*, 15471–15477.
(10) Hirsimäki, M.; Lampimäki, M.; Lahtonen, K.; Chorkendorff, I.; Valden, M. *Surf. Sci.* **2005**, *583*, 157–165.
(11) Bagot, P. A. J.; Cerezo, A.; Smith, G. D. W.; de Bocarme, T. V.; Godfrey, T. J. *Surf. Interface Anal.* **2007**, *39*, 172–177.
(12) Tao, F.; Grass, M. E.; Zhang, Y.; Butcher, D. R.; Renzas, J. R.; Liu, Z.; Chung, J. Y.; Mun, B. S.; Salmeron, M.; Somorjai, G. A. *Science* **2008**, *322*, 932–934.
(13) Nerlov, J.; Chorkendorff, I. *J. Catal.* **1999**, *181*, 271–279.
(14) Nerlov, J.; Sckerl, S.; Wambach, J.; Chorkendorff, I. *Appl. Catal., A* **2000**, *191*, 97–109.
(15) Knudsen, J.; Nilekar, A. U.; Vang, R. T.; Schnadt, J.; Kunkes, E. L.; Dumesic, J. A.; Mavrikakis, M.; Besenbacher, F. *J. Am. Chem. Soc.* **2007**, *129*, 6485–6490.
(16) Schumacher, N.; Boisen, A.; Dahl, S.; Gokhale, A. A.; Kandoi, S.; Grabow, L. C.; Dumesic, J. A.; Mavrikakis, M.; Chorkendorff, I. *J. Catal.* **2005**, *229*, 265–275.
(17) Schumacher, N.; Andersson, K.; Grabow, L. C.; Mavrikakis, M.; Nerlov, J.; Chorkendorff, I. *Surf. Sci.* **2008**, *602*, 702–711.
(18) Schumacher, N.; Andersson, K. J.; Nerlov, J.; Chorkendorff, I. *Surf. Sci.* **2008**, *602*, 2783–2788.

 10.1021/ja8089087 CCC: $40.75

structure. The earlier density functional theory (DFT) study[15] indicated increased Pt−CO bonding when Cu is present in the first layer, similar to what is observed for other coinage/Pt-group metal systems.[19−22] Here we prove Cu surface segregation induced by a drastically stronger Pt−CO bond in the self-organized CO/CuPt SA structure. The results are confirmed by extended DFT calculations.

2. Methods

The ultrahigh vacuum (UHV)/high-pressure cell (HPC) system combined with a polarization modulation infrared reflection absorption spectroscopy (PM-IRAS) setup has been described elsewhere.[17] PM-IRAS is an FT-IR method utilizing s- and p-polarized radiation to distinguish between adsorbed and gas-phase molecules. Cu was deposited at a rate of ∼0.2 atomic layers/min on Pt(111) held at 425 K. No surface contaminants were observed by X-ray photoelectron spectroscopy (XPS), He^+ ion scattering spectroscopy (ISS), low-energy electron diffraction (LEED), or IR before, during, or after CO treatments. In particular, possible Ni impurities from $Ni(CO)_4$[14] were consistently measured to be ≤0.005 monolayer (ML) as judged by XPS.

The DFT calculations were performed using the DACAPO code.[23] Electron−ion interactions were described by ultrasoft pseudopotentials[24] within a plane-wave basis with a cutoff energy of 350 eV. Electron exchange and correlation effects were described by the RPBE[23] generalized gradient approximation functional. The electron density of the valence states was obtained by a self-consistent iterative diagonalization of the Kohn−Sham Hamiltonian with Pulay mixing of the densities.[25] The occupation of the one-electron states was calculated using an electronic temperature of $k_BT = 0.1$ eV (0.01 eV for CO in vacuum); all of the energies were extrapolated to $T = 0$ K. The surface [$(\sqrt{3} \times \sqrt{3})R30°$ unit cell] was modeled by a periodic array of four layers separated by more than 10 Å of vacuum. Adsorption energies were converged to within ∼0.05 eV with respect to slab thickness; energy differences are expected to be even more accurate. The energetics of Cu in the second layer relative to the bulk was evaluated using $(2\sqrt{3} \times \sqrt{3})R30°$ periodically repeated four-layer slabs with and without vacuum separation. For the surface calculations, the top two layers including CO were allowed to fully relax during geometry optimizations, and for the bulk calculations, all of the atoms were relaxed. Monkhorst−Pack grids with dimensions 3 × 3 × 1, 2 × 3 × 1, and 3 × 8 × 4 were used for sampling the Brillouin zones of the surface $(\sqrt{3} \times \sqrt{3})R30°$, surface $(2\sqrt{3} \times \sqrt{3})R30°$, and bulk $(2\sqrt{3} \times \sqrt{3})R30°$ structures, respectively. The experimentally determined Pt lattice parameter of 3.92 Å was used throughout.

3. Results and Discussion

Initially, a CuPt NSA was prepared by depositing one atomic layer of Cu ($\theta_{Cu} = 1$ ML) on Pt(111) and annealing to 800 K. XPS, ISS, and LEED analyses supported prior findings[15] that Cu is preferentially located in the second layer. The NSA's stability against CO adsorption was tested by a CO treatment in an HPC. The sample was exposed to CO at a pressure of 2 mbar for 10 min at various sample temperatures and then cooled to room temperature (RT) over 10 min in the CO, after which the CO was evacuated.

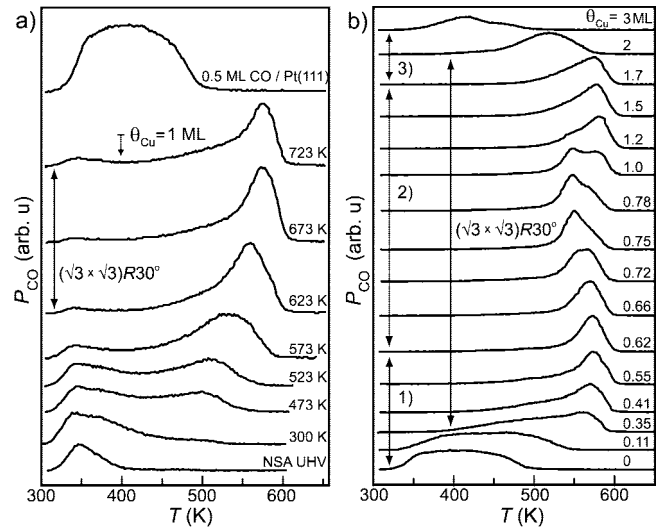

Figure 2. CO TPD spectra (2 K/s) recorded under UHV after various sample treatments. (a) Reference and post-treatment TPDs for a 1 ML Cu/Pt(111) NSA exposed to CO at 2 mbar for 10 min at the temperatures shown in the figure. Bottom and top traces (reference TPDs): NSA UHV (no high-pressure exposure) and 0.5 ML of CO on clean Pt(111), respectively. (b) TPDs after 2 mbar CO treatment at 673 K for varying amounts of Cu as displayed in the figure. Also marked in the figure are three distinctive regions (1, 2, and 3) and observations of a $(\sqrt{3} \times \sqrt{3})R30°$ LEED pattern, as discussed in the text.

We show in Figure 2 the CO temperature-programmed desorption (TPD) spectra obtained under UHV before and after the HPC CO treatments. First, for adsorption of CO under UHV conditions, we compare the CO desorption from the CuPt NSA (Figure 2a, bottom trace) to that from pure Pt(111) (Figure 2a, top trace). Evidently, less CO is adsorbed at RT and binds significantly more weakly (i.e., desorbs at a much lower temperature) on the CuPt NSA. This agrees well with prior findings.[15]

Exposing the CuPt NSA surface to 2 mbar CO at 300 K results only in very small changes, (see Figure 2a). However, after treatment at temperatures in the range 473−723 K in the 2 mbar CO, the CO desorption peaks are located at temperatures as high as 580 K. For $T_{treatment} \geq 623$ K, the CO coverages are large and saturated at 0.3−0.33 ML. The results demonstrate drastically increased CO binding energy, even compared with that on pure Pt(111), and we conclude that the CuPt NSA surface is not stable but undergoes changes when in the CO environment at elevated temperatures. The changes are reversible upon desorption of the CO under UHV by annealing to 673−800 K, which regenerates the NSA and its CO adsorption characteristics (Figure 2a, bottom).

On the basis of the TPD spectra measured after HPC CO treatments at 673 K for samples with varying θ_{Cu} in the range 0−3 ML (Figure 2b), three different regions were established: (1) $\theta_{Cu} < 0.62$ ML, (2) $\theta_{Cu} = 0.62-1.7$ ML, and (3) $\theta_{Cu} > 1.7$ ML. The starting surfaces were as-deposited Cu on Pt(111). The treatment temperature, 673 K, was chosen on the basis of the findings in Figure 2a and is well above the onset for Cu diffusion into Pt.[17] The high-temperature CO desorption feature at 570−580 K is fully developed at 0.62 ML (no traces of lower temperature states) and remains for a Cu content of up to 1.7 ML (region 2) before systematically shifting to lower temperature in region 3. An observed deviation at 0.72−1.2 ML of

(19) Hager, T.; Rauscher, H.; Behm, R. J. *Surf. Sci.* **2004**, *558*, 181–194.
(20) Gonzalez, S.; Illas, F. *Surf. Sci.* **2005**, *598*, 144–155.
(21) Sakong, S.; Mosch, C.; Gross, A. *Phys. Chem. Chem. Phys.* **2007**, *9*, 2216–2225.
(22) Inderwildi, O. R.; Jenkins, S. J.; King, D. A. *Surf. Sci.* **2007**, *601*, L103–L108.
(23) Hammer, B.; Hansen, L. B.; Nørskov, J. K. *Phys. Rev. B* **1999**, *59*, 7413.
(24) Vanderbilt, D. *Phys. Rev. B* **1990**, *41*, 1510.
(25) Kresse, G.; Furthmuller, J. *Comput. Mater. Sci.* **1996**, *6*, 15.

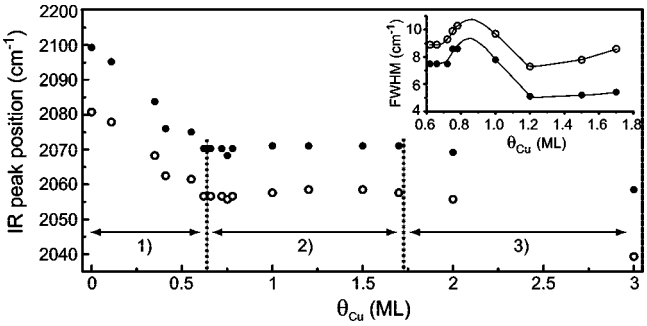

Figure 3. Correlation between atop-CO IR peak positions and (inset) fwhm's for the samples in Figure 2b during the 2 mbar CO/673 K treatment (○) and under UHV at 300 K after the treatment (●). Lines serving as guides to the eye are shown in the inset.

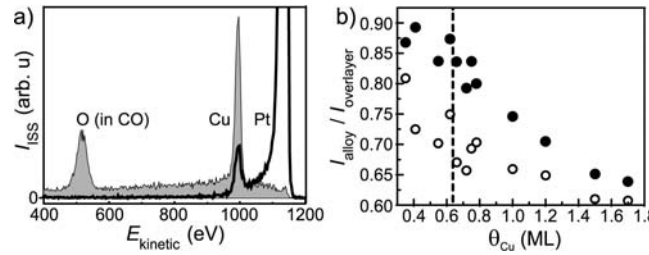

Figure 4. ISS and XPS spectra showing Cu surface segregation induced by CO adsorption. (a) ISS after 2 mbar CO/673 K treatment of a 0.67 ML Cu/Pt(111) sample (gray) and the corresponding NSA (black). (b) XPS Cu 2p/Pt 4d ratio (relative to the case of as-deposited Cu) for the 2 mbar CO/673 K treated samples in Figure 2b before TPD (●) and the corresponding NSAs after TPD (○). In (b), the line at ~0.62 ML of Cu marks an apparent Cu saturation in the first layer of the surface alloy (●).

Cu using the described sample-preparation procedure, with a ~550 K CO TPD peak, is discussed later in connection with our XPS results. In region 2, the saturation coverage of CO in the 570−580 K peak is very close to $^1/_3$ ML (0.36 ± 0.02 ML), as for the 1 ML CuPt NSA in Figure 2a.

Distinct surface changes accompanied the high-temperature desorption features in Figure 2. At 0.35 ML of Cu, the high-temperature desorption feature appeared (Figure 2b), accompanied by a weak, broad, diffuse $(\sqrt{3} \times \sqrt{3})R30°$ LEED pattern that was very sharp and intense at ~0.7 ML of Cu and further observed at up to 2 ML of Cu. The $(\sqrt{3} \times \sqrt{3})R30°$ LEED pattern was also clearly observed for the 1 ML NSA sample in Figure 2a for CO treatments at $T \geq 623$ K. Furthermore, whereas atop-adsorbed CO (~2100−2050 cm^{-1}) always was observed in IR spectra, bridge-bonded CO (~1855 cm^{-1}) was observed neither during nor after HPC CO treatment for any CuPt alloy surface with $\theta_{Cu} \geq 0.35$ ML.

When PM-IRAS was used to compare IR peak characteristics for atop-site-adsorbed CO (see Figure 3) the correlation between our in situ (2 mbar CO, 673 K) and ex situ (UHV, RT) data was found to be very high. The nearly constant shifts in IR peak position and fwhm broadening for the in situ data with respect to the ex situ data are most likely due to the temperature difference. The three regions 1, 2, and 3 already identified in the TPD data are strongly reflected in the IR data. From observations of a peak in fwhm in the range 0.72−1.2 ML of Cu, it is also apparent that the ~550 K CO TPD peak is reflected in the IR data. The in situ and ex situ IR peak positions and fwhm's for CO treatments of the sample with 1 ML of Cu at $T \geq 623$ K (Figure 2a) were identical (within 4 cm^{-1}) to those in region 2 of Figure 3. All of the results obtained under UHV at 300 K after HPC CO treatment strongly reflect the in situ surface characteristics during treatment.

Cu surface segregation was found to be associated with the CO-induced surface structural changes for the samples in Figure 2 by using ISS (1.2 keV He^+, $\theta = 125°$) and XPS to characterize the elemental composition in the topmost surface layer and near-surface region, respectively. In Figure 4a, the ISS spectrum after treatment of a sample with $^2/_3$ ML of Cu for 10 min at 673 K in 2 mbar CO is compared with the spectrum obtained from the corresponding NSA (~1 s anneal at 673 K under UHV). For the NSA, the Cu content in the top surface layer is very small (0.03 ML) and the Pt signal is dominant. Contrary to the expected diffusion of Cu into Pt at 673 K, Cu surface segregation due to the HPC CO treatment leads to a large ISS intensity for Cu (0.13 ML), and surface Pt is barely observed, being blocked by adsorbed CO. The maximum amount of Cu in the top surface layer observed for the samples in Figure 2 according to ISS was 0.14 ML. However, the actual coverage should be much higher, since experiments for 0.5 ML of CO on Pt(111) showed that adsorbed CO also blocks remaining surface sites from He^+ ion impingement.

The Cu surface segregation induced by the CO adsorption was also confirmed by XPS (see Figure 4b). Although there is a degree of scatter in the data, in every case the Cu content in the near-surface region after 10 min at 2 mbar CO and 673 K is significantly larger than for the corresponding NSA (~1 s anneal at 673 or 800 K under UHV). Very similar results were obtained for $T_{treatment} \geq 523$ K in Figure 2a. For the 0.35 ML ≤ $\theta_{Cu} \leq 0.62$ ML HPC CO-treated samples, the Cu signal is a nearly constant fraction (0.84−0.9) of the initial amount of Cu deposited, and this signal drops significantly for larger θ_{Cu}. Upon correlation of the XPS data with the ISS results showing large Cu amounts in the first layer, the findings indicate that essentially all of the Cu remains in the first layer up to ~$^2/_3$ ML, after which the superfluous Cu starts to distribute itself in deeper layers (hence the drop in relative intensity). The IR and TPD results suggest heterogeneity in the CO adsorption site, with some Cu in the second layer in the range 0.72−1.2 ML of Cu. The heterogeneity may be due to a small transition period after the onset of the Cu bulk migration at $\theta_{Cu} > {}^2/_3$ ML suggested by XPS, where some superfluous Cu still remains in the second layer, leading to the somewhat lowered (~25 K) CO desorption temperature in this region. At $\theta_{Cu} > 1.7$ ML, the origin of the lowered CO adsorption energy is likely a large second-layer Cu population even after the HPC CO treatment.

Although Cu diffusion to the first layer is endothermic,[15] the observed drastic increase in CO binding energy more than compensates for the endothermicity. This was established using DFT calculations. A $(\sqrt{3} \times \sqrt{3})R30°$ unit cell was used, and Cu was restricted to the first and second layers for total Cu amounts of $^1/_3$, $^2/_3$, 1, $^4/_3$, and $^5/_3$ ML with and without $^1/_3$ ML of CO adsorbed on atop Pt sites. Stabilities were calculated relative to Cu in the bulk and CO adsorption on clean Pt(111), as shown in Table 1.

For the clean surfaces (no CO adsorbed), $^2/_3$ ML of Cu in the second layer is the most stable, and Cu diffusion from the second to the first layer is generally endothermic by 0.3−0.4 eV. With $^1/_3$ ML of CO adsorbed atop surface Pt, the situation is very different: Cu surface migration to generate $^2/_3$ ML of Cu in the first layer is now most favorable. Clearly, there is a driving force toward having $^2/_3$ ML of Cu in the first layer when CO is adsorbed atop the remaining surface Pt sites. As Table 1 shows, the origin of the exothermicity is the vastly increased

Table 1. DFT Results for Cu Segregation Energies ($\Delta E_{segr,Cu}$) with and without $^1/_3$ ML of CO Adsorbed atop Pt and Differential ($\Delta E_{ads,CO}$) and Absolute ($E_{ads,CO}$) CO Adsorption Energies[a]

Cu content (ML)	distribution in 1st and 2nd layers (1st:2nd)	clean surface $\Delta E_{segr,Cu}$ (eV)	$\Delta E_{ads,CO}$ ($E_{ads,CO}$) (eV)	with CO adsorbed $\Delta E_{segr,Cu}$ (eV)
0	Pt_3Cu_0:Pt_3Cu_0	−	0 (−1.38)	−
$^1/_3$	Pt_3Cu_0:Pt_2Cu_1	−0.17	+0.08 (−1.30)	−0.09
	Pt_2Cu_1:Pt_3Cu_0	+0.13	−0.22 (−1.60)	−0.09
$^2/_3$	Pt_3Cu_0:Pt_1Cu_2	**−0.36**	+0.21 (−1.17)	−0.15
	Pt_2Cu_1:Pt_2Cu_1	0.00	−0.04 (−1.42)	−0.04
	Pt_1Cu_2:Pt_3Cu_0	+0.32	−0.64 (−2.03)	**−0.32**
1	Pt_3Cu_0:Pt_0Cu_3	−0.11	+0.23 (−1.16)	+0.12
	Pt_2Cu_1:Pt_1Cu_2	−0.09	+0.19 (−1.20)	+0.09
	Pt_1Cu_2:Pt_2Cu_1	+0.36	−0.37 (−1.75)	−0.01
$^4/_3$	Pt_2Cu_1:Pt_0Cu_3	+0.14	+0.37 (−1.02)	+0.51
	Pt_1Cu_2:Pt_1Cu_2	+0.50	−0.19 (−1.58)	+0.31
$^5/_3$	Pt_1Cu_2:Pt_0Cu_3	+0.85	+0.07 (−1.31)	+0.92

[a] Cu in the bulk and CO adsorption on clean Pt(111) were used as reference states. The most stable configurations are highlighted in bold print.

Pt−CO bond strength when $^2/_3$ ML of Cu is present in the first layer. The calculations also show weakening of the Pt−CO bond with increasing Cu content in the second layer. Both results strongly support our experimental findings, and the 0.6−0.85 eV increase in CO binding energy in going from the NSA to the SA with $^2/_3$ ML of Cu agrees very well with the value of 0.7 eV derived from our TPD data (peak positions, 350 vs 580 K; heating rate, 2 K/s; assumed first-order desorption and pre-exponential factor, $\upsilon \approx 10^{14}$ s^{-1}).[27]

For the very important case of $^2/_3$ ML of Cu and $^1/_3$ ML of adsorbed CO, the calculated higher stability of the CuPt SA compared with Cu in the bulk with CO adsorption on clean Pt(111) is nearly equal to the free-energy difference (ΔG). This is true because ΔG in this case can be taken as the enthalpy difference ΔH, since the estimated CO equilibrium coverages at 2 mbar CO and 673 K are very similar (close to $^1/_3$ ML) on Pt(111) (∼0.4 ML, from ref 26) and the CuPt SA (0.36 ± 0.02 ML).

We note that the results with adsorbed CO in Table 1 can explain the $\theta_{Cu} > \sim^2/_3$ ML onset of bulk migration of Cu indicated by our XPS data. In comparison with the $\theta_{Cu} = ^2/_3$ ML case, situations with higher Cu content in the top two layers are significantly less stable, leading to a significant Cu bulk migration driving force.

(26) Davies, J. C.; Nielsen, R. M.; Thomsen, L. B.; Chorkendorff, I.; Logadóttir, Á.; Lodziana, Z.; Nørskov, J. K.; Li, W. X.; Hammer, B.; Longwitz, S. R.; Schnadt, J.; Vestergaard, E. K.; Vang, R. T.; Besenbacher, F. *Fuel Cells* **2004**, *4*, 309–319.

(27) Chorkendorff, I.; Niemantsverdriet, J. W. *Concepts of Modern Catalysis And Kinetics*; Wiley-VCH: Weinheim, Germany, 2003.

Finally, although we have no atomistic picture of the actual mechanism for Cu migration in and out, the kinetic barriers are apparent in our data. The interdiffusion of Cu and Pt becomes significant at ∼460 K,[17] and this is also approximately where both the formation and breakup of the stable CO-induced surface alloy start to occur (see Figure 2). In forming the SA from the NSA, the interdiffusion mobility allows for Cu migration events to the first layer, and this Cu can then be trapped in the new low-energy SA configuration with CO adsorbed.

4. Summary and Conclusions

It is clear that CO adsorption at elevated pressures and temperatures on a CuPt near-surface alloy induces a large Cu surface segregation, generating a novel CuPt surface alloy to which CO binds very strongly, even compared with pure Pt(111). The Cu content needed for saturation of the SA is $\sim^2/_3$ ML of Cu, leading to a CO saturation coverage of $\sim^1/_3$ ML. The sharp CO TPD spectrum compared with that of pure Pt(111), the observed $(\sqrt{3} \times \sqrt{3})R30°$ LEED pattern, and the IR-peak red shift and narrow fwhm strongly suggest a significantly reduced lateral (repulsive) interaction between CO molecules adsorbed atop Pt sites and hence a well-ordered surface with well-defined, well-dispersed, and isolated Pt sites. DFT calculations reproduce the experimental observations and confirm that the vastly increased Pt−CO binding energy with $^2/_3$ ML of Cu in the first layer of Pt rationalizes the observed Cu surface segregation.

An important consequence of our results is that they add to the promise of using molecular adsorbate-induced surface changes as a tool for selective and dynamical engineering of alloy surfaces.[13,14] In view of the earlier indications of increased Pt-group metal bonding to CO when Cu or Ag is present in the first layer with a Pt-group metal,[19−22] our results for the CuPt system at elevated temperatures and CO pressures, where a novel stable CO-induced surface alloy forms, likely extend to a wide variety of coinage (Cu, Ag)/Pt-group bimetallic surface alloys.

Acknowledgment. CINF is sponsored by The Danish National Research Foundation, and CAMD is funded by the Lundbeck Foundation. K.J.A. acknowledges a postdoctoral grant from the Wenner-Gren Foundations, and F.C.-V. acknowledges support from the Strategic Electrochemistry Research Center. Dr. Martin Johansson, CINF, is gratefully acknowledged for helpful discussions.

JA8089087